Nanoscale

Cite this: *Nanoscale*, 2012, **4**, 5989

www.rsc.org/nanoscale

PAPER

Slip corona surrounding bilayer graphene nanopore†

Liang Qi,[a] Yunwei Mao[b] and Ju Li*[abc]

Received 5th June 2012, Accepted 11th July 2012
DOI: 10.1039/c2nr31405c

The electronic and magnetic properties of bilayer graphene (BLG) depend on the stacking order between the two layers. We introduce a new conceptual structure of "slip corona" on BLG, which is a transition region between A–A stacking close to a nanopore composed of bilayer edges (BLEs) and A–B stacking far away. For an extremely small nanopore (diameter $D_{pore} < \sim 5$ nm), both atomistic simulations and a continuum model reach consistent descriptions on the shape and size of this "corona" (diameter ~50 nm), which is much larger than the width of the typical dislocation core (~1 nm) in 3D metals or the nanopore itself, due to the weak van der Waals interactions and low interlayer shear resistance between two adjacent layers of graphene. The continuum model also suggests that the width of this "corona" from the BLE to the A–B stacking area would increase as D_{pore} increases and converge to ~40 nm when D_{pore} is more than ~80 nm. This large stacking transition region provides a new avenue for tailoring BLG properties.

I. Introduction

Compared with monolayer graphene (MLG) which is a zero band-gap semimetal, bilayer graphene (BLG) has attracted a lot of attention recently for possible device applications since it possesses a band gap in the presence of an external electric field.[1,2] The properties of BLG were interpreted mostly under the assumption that the stacking of two graphene layers takes the form of an A–B or Bernal stacking as shown in Fig. 1(a), the most common stacking order in graphite.[3–6] However, in 2009, it was found by Suenaga and Iijima *et al.* through high-resolution transmission electron microscopy (HRTEM),[7] confirmed by Huang and Li *et al.*[8,9] that bilayer edges (BLEs) or "half-nanotubes"[10] as shown in Fig. 1(b) can change the stacking of BLG from A–B to A–A, where the two layers are stacked on top of one another (Fig. 1(c)). Because the electronic and magnetic properties of BLG depend on the stacking order, this A–A stacking can result in abnormal Berry's phases and quantum Hall effects.[9,11–14] BLE (half-nanotube) has no dangling bonds and similar chemical inertness to a full nanotube at room temperature, because fundamentally it is formed by folding graphene like full nanotubes, but rotating graphene by π instead of 2π. Unlike full nanotubes though, BLE has highly monodisperse folding chirality/edge inclination[7,8] (pure zigzag or armchair only) due to the π-rotation.[15] For device applications, BLEs or half-nanotubes are advantageous because their atomic structure is well-defined, with atomically sharp and very straight edges experimentally, in contrast to the atomically rough monolayer edge (MLE) with irregular shapes.[15] Thus, BLE on BLG provides a new avenue for graphene-based nanodevices[16] with exceptionally stable and well-defined edges to yield uniform and controllable device behavior.[10] However, this integration brings an interesting new phenomenon regarding the *stacking order*: BLEs prefer A–A stacking due to the atomic structures of 1D edge lines,[9] while infinite BLG prefers A–B stacking due to the van der Waals interaction proportional to the 2D area, so a stacking transition from A–A near BLEs to A–B far away should happen on relatively large BLG with BLEs.

The nanopore on BLG with BLEs as pore edges, as shown in Fig. 1(d), is a perfect system to study this stacking-order transition because of geometric simplicity and possible applications. Graphene nanopores are structures of interest for energy storage[17,18] and molecule/ion selection;[19,20] they can also be used for sensing and detection, like DNA translocation sequencing when graphene is used as the trans-electrode membrane.[21–24] Most nanopores exist on multiple layers of graphene. With BLEs forcing the A–B to A–A transition near the pore that changes electronic and magnetic properties, details of the transition will influence electronic detection of DNA and other potential applications. Thus, it is necessary to obtain a comprehensive and quantitative understanding of the stacking-order transition associated with the BLG nanopore as shown in Fig. 1(d), which is the main task of this paper. This stacking-order "topological

[a]*Department of Nuclear Science and Engineering, Massachusetts Institute of Technology, Cambridge, Massachusetts 02139, USA. E-mail: liju@mit.edu*
[b]*Center for Advancing Materials Performance from the Nanoscale (CAMP-Nano), State Key Laboratory for Mechanical Behavior of Materials, and Frontier Institute of Science and Technology, Xian Jiaotong University, Xian 710049, China*
[c]*Department of Materials Science and Engineering, Massachusetts Institute of Technology, Cambridge, Massachusetts 02139, USA*
† Electronic supplementary information (ESI) available. See DOI: 10.1039/c2nr31405c

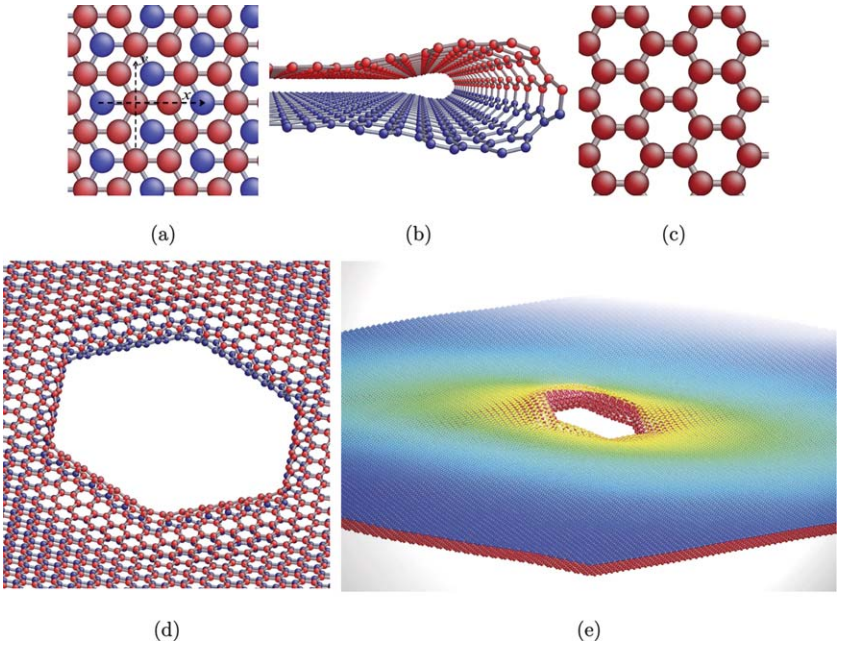

Fig. 1 (a) Atomic structure of BLG in A–B stacking from top view; from (a) to (d) red and blue atoms are at the top and bottom layers, respectively. (b) Atomic structure of a zigzag BLE with A–A stacking BLG near the edge. (c) Top view of BLG with A–A stacking so that two layers totally overlap. (d) Hexagonal nanopore on BLG with BLE as edges. (e) Conceptual illustration of a diffuse slip displacement field between two graphene layers close to a BLG nanopore like (d). Different colors of the top layer indicate the magnitude of the relative slip distance between two layers so that red/blue color on the top layer means A–A/A–B stacking, respectively.

defect" is similar to the concept of dislocation in solid mechanics, where the finite lattice disregistry in the dislocation core gradually decays to zero far from the core.[25] However, different from normal dislocation that is 1D line defect in the 3D lattice, our new structure produces a 2D field of slip displacement between the two graphene layers relative to normal A–B stacking (considered to be the reference, or slip $\boldsymbol{s} = 0$). This field surrounding the BLG nanopore as shown in Fig. 1(e), similar to the corona surrounding the sun, is named "slip corona" on multilayer graphene.

To simplify the mechanical analysis, we first assume the pore is infinitesimal and approximate the pinning effect of the nanopore as fixing just one atom pair from the top and bottom layers to be A–A, with the stacking order relaxing to A–B far away from this point, which can be named as a "point-constraint" case. Setting this point as the origin ($\boldsymbol{x} = 0$), slip displacement $\boldsymbol{s}(\boldsymbol{x})$ can be defined as

$$\boldsymbol{s}(\boldsymbol{x} = 0) = \mathbf{BA},\ \boldsymbol{s}(\boldsymbol{x} \to \infty) = 0 \qquad (1)$$

We will solve $\boldsymbol{s}(\boldsymbol{x})$ using both atomistic simulations and a continuum Peierls–Nabarro (PN) model of the dislocation core,[26,27] which is based on the interlayer force obtained from generalized stacking fault (GSF) energy calculations.[26–28] Both methods output almost the same displacement fields between the two layers in the transition region, which behaves like a diffuse and displacement-decaying "corona" surrounding the center with a diameter of ~50 nm. This 2D slip corona is much larger than the dimension of the typical dislocation core in 3D solids, which is just several Å or 1–2 nm in width.[29,30] We extend the analyses to real atomic structures of the hexagonal BLE nanopore, shown in Fig. 1(d), and similar slip corona fields are obtained. At the end of this paper, we use the continuum model to numerically solve the displacement fields of BLE nanopores with various sizes and analyze how the size of the slip corona changes correspondingly.

II. Methods

A. Molecular dynamics simulations

Molecular dynamics (MD) simulations were performed by a LAMMPS Molecular Dynamics simulator with adaptive intermolecular reactive empirical bond order (AIREBO) potential,[31] where the torsion term was included. For the "point-constraint" case, we constructed 2D BLG in periodic square supercells with different side lengths (50 nm × 50 nm, 100 nm × 100 nm and 500 nm × 500 nm). In the supercell, there is one-to-one correspondence with atoms in the top and bottom layers. The coordination system is defined in Fig. 1(a) (x-axis is along the armchair edge; y-axis is along the zigzag edge). The ideal A–B stacking is taken as the reference system, so the displacement between two layers is defined as zero everywhere in a perfect A–B stacking BLG. On the other hand, for one atom pair from the top and bottom layers in A–A stacking, the displacement is a carbon–carbon bond length A_0 along the x-axis, which is 1.40 Å according to empirical interatomic potential,[31] and 0 Å along the y-axis. In the center of our investigated supercells, one atom pair from the top and bottom layers was always fixed as A–A stacking to simulate that there was an infinitesimal BLG nanopore with infinitely high stiffness, so $\boldsymbol{s}(x = 0,\ y = 0) = 0$ would not change under external stress. Initially, a gradually

varying trial $\boldsymbol{s}(x, y)$ was added to transform this A–A stacking in the center to A–B stacking far away. To obtain the equilibrium distribution of the displacement field under this constraint, conjugated gradient (CG) minimization was applied first for the whole supercell while fixing A–A stacking for the atom pair at center, followed by MD simulations with the same constraint at 50 K for 100 picoseconds, and then followed by CG minimization again. All atoms except the center atom pair were relaxed in all three directions x, y, z. With the equilibrium configuration, the displacement fields $\boldsymbol{s}(x,y) = [u(x,y),v(x,y)]$, where u/v is the displacement along x/y-axis defined according to the reference system mentioned above, were obtained by calculating the displacement vector of each atom at the top layer relative to the atom in the corresponding pair at the bottom layer.

In addition, we built 2D BLG periodic square supercells (50 nm × 50 nm and 100 nm × 100 nm) with the hexagonal nanopore as shown in Fig. 1(d). On this nanopore each edge is a zigzag BLE and the length of each edge is 2.9 nm. All the atoms on the BLE are in sp^2 bonding state with three nearest neighbors, and there is a decagon on each corner of the edge intersections. Then we performed the same MD calculations as the above procedures, except that all the atoms in the supercell were relaxed. The displacement fields $\boldsymbol{s}(x,y) = [u(x,y),v(x,y)]$ were also obtained based on the equilibrium configurations.

B. Continuum model

The results from direct atomistic simulation depend on the accuracy of empirical interatomic potential. Thus, it is instructive also to build a continuum model of this 2D slip corona that can output the analytical description of this displacement field. As in the PN model, there are two types of forces involved in the slip corona. One is the in-plane elastic force in monolayer graphene due to $\nabla\boldsymbol{s}$; the other is the nonlinear glue force between two layers due to the GSF.[26,27] At equilibrium, the net force on each point is zero, so the governing equation can be built based on this requirement. For the elastic force, we regard monolayer graphene as an isotropic medium which can be described by two parameters, E, the Young's modulus and ν, the Poisson ratio. For the interlayer glue force, it depends on the interaction potential between two layers. So we need to calculate GSF energy for BLG, also called the γ-surface, which is a 2D periodic energy surface $\gamma(\boldsymbol{s})$ that describes the variation of interlayer energy due to rigid shifts between the top and bottom layers.[28] Thus BLG was built in a 5.80 × 5.86 nm^2 supercell with 2688 atoms and molecular static calculations were performed based on AIREBO potential.[31] Rigid displacements between two graphene layers were applied and CG minimization was used to relax all atoms only along the z-axis. GSF for a rigid shift $\boldsymbol{s}$, $\gamma(\boldsymbol{s})$, is calculated as

$$\gamma(\boldsymbol{s}) = (E_{\mathrm{n}}(\boldsymbol{s}) - E_{\mathrm{n0}})/A_{\mathrm{s}} \quad (2)$$

here $E_{\mathrm{n}}(\boldsymbol{s})$ and E_{n0} are the energies of the supercell with rigid shift $\boldsymbol{s} = [u,v]$ and the supercell with perfect A–B stacking, respectively; A_{s} is the area of supercell.

To build a mathematical model for an analytic description of the displacement field, we need to get an approximate analytical expression of GSF based on the above atomic calculations, from which we can give an analytical expression of the glue force between two layers in BLG. Because monolayer graphene is just one atom-layer in thickness, technically, we consider the force between two layers as the body force. Setting t as the effective thickness of the graphene monolayer, the force along x-axis and y-axis can be expressed as $f_x(u, v) = -\partial_u\gamma/t$ and $f_y(u, v) = -\partial_v\gamma/t$. If we do not take wrinkles and ripples of graphene into account[32] and regard this model as a plane stress problem,[33] we can write down the governing equations as

$$\begin{cases} \dfrac{\partial^2 u}{\partial x^2} + \dfrac{1-\nu}{2}\dfrac{\partial^2 u}{\partial y^2} + \dfrac{1+\nu}{2}\dfrac{\partial^2 v}{\partial x \partial y} - \dfrac{2(1-\nu^2)}{E}(-\partial_u\gamma/t) = 0 \\ \dfrac{\partial^2 v}{\partial y^2} + \dfrac{1-\nu}{2}\dfrac{\partial^2 v}{\partial x^2} + \dfrac{1+\nu}{2}\dfrac{\partial^2 u}{\partial x \partial y} - \dfrac{2(1-\nu^2)}{E}(-\partial_v\gamma/t) = 0 \\ u(x,y), v(x,y) \to 0 \quad \text{when } |x| \to \infty \quad \text{or } |y| \to \infty \\ u(x,y) = B_1(x,y); v(x,y) = B_2(x,y) \quad \text{when } (x,y) \in \partial\Omega \end{cases} \quad (3)$$

Ω means the domain of the equations; here the domain is infinite. $\partial\Omega$ means the finite-value border of the domain. $B_1(x, y)$ and $B_2(x, y)$ are two boundary value functions which are given according to detailed structures. For simplification, here we just build the continuum model of the "point-constraint" case, so $\partial\Omega$ is the point located at the fixed pair, which is (0,0) in our reference, and the boundary value functions are $B_1(0, 0) = A_0$ (carbon–carbon bond length) and $B_2(0, 0) = 0$ in this situation. The solutions of these governing equations are shown in Section III B.

III. Results and discussions

A. MD simulations of point-constraint case

The displacement fields of u and v in a 50 nm × 50 nm supercell for the "point-constraint" case are plotted from top view in Fig. 2. The results of a 100 nm × 100 nm supercell are also plotted in the ESI, Fig. S1,† which are almost the same as those in the smaller supercell. It shows that most displacements occur along the x-axis surrounding the fixed center in the shape of an ellipse with the size of tens of nanometers. u decreases from 1.40 Å (A–A stacking) at the center to ~0 Å (A–B stacking) far from the center. On the other hand, the displacements along the y-axis are very small (−0.05 Å < v < +0.05 Å) and can be divided into four different sections with different signs; in each section, it behaves like a liquid-drop shape; the magnitude of v decreases from the maximum in the center (~0.05 Å) to 0 far from it. Beside displacements along the x and y directions, there are also undulations along the z-axis so that there are many ripples on each layer of BLG with wavelength of several nanometers,[32] thus most atom pairs have total displacements oscillating near the ideal value of A–B stacking (0 Å here). However, such ripples would not affect x–y displacement fields significantly except for v far from the center, where the magnitudes of v are very small (between −0.01 Å and 0.01 Å).

To investigate the shape and size of the displacement field in a more quantitative way, the total displacement of each atom pair, $d \equiv \sqrt{u^2 + v^2}$, is projected on both x and y-axes, respectively, and plotted in Fig. 2(c)–(e) for different supercells. First, it shows that the maximum of d decreases from 1.40 to ~0 Å

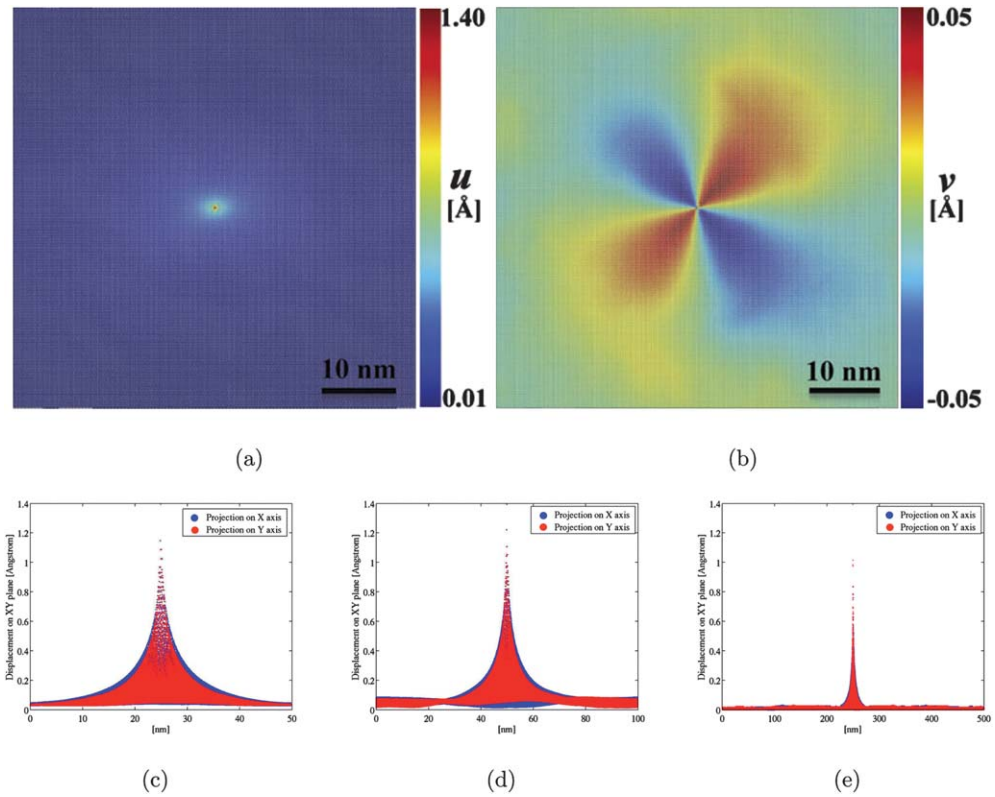

Fig. 2 (a) and (b) Displacement fields of BLG along the x-axis, u, and along the y-axis, v, in a 50 nm × 50 nm supercell with one central atom pair fixed as A–A stacking. From (c) to (e) total displacements ($d = \sqrt{u^2 + v^2}$) projected on both x and y-axes in (c) 50 nm × 50 nm, (d) 100 nm × 100 nm and (e) 500 nm × 500 nm supercell, respectively.

smoothly, behaving like a displacement-decaying "volcano". Second, it decays a little bit more quickly along the y-axis than the x-axis, indicating that the contours of the displacement field are elliptically shaped. Third, the size of such decaying fields can be determined: in Fig. 2(c), the maximum d keeps decreasing until the boundaries of the 50 nm × 50 nm supercell; the non-zero value of d at the boundary comes from the ripple structure mentioned above. In Fig. 2(d), the slope of the maximum d becomes almost zero when it is ~25 nm away from the center, beyond which d oscillates around ~0 Å so that BLG behaves like A–B stacking and the oscillations originate from the ripples on two layers; in Fig. 2(e), such transition of slopes for the maximum d also occurs at ~25 nm away from the center. From these convergent calculations, it can be estimated that the transition region of the displacement fields under single-point constraint of A–A stacking in BLG has a diameter of ~50 nm, much larger than the typical dislocation core width (few nm) in 3D solids.[29,30] It is also significantly bigger than most graphene nanopores themselves.

B. A continuum model of point-constraint case

GSF $\gamma(\boldsymbol{s})$ of BLG is obtained from eqn (2) based on AIREBO potential and the result is plotted in Fig. 3(a), where GSF behaves as energy-increasing circular contours surrounding the displacement vector corresponding to A–A stacking of BLG. The maximum stacking fault energy at A–A stacking is ~5 mJ m^{-2}, much smaller than the typical metallic system (~160 mJ m^{-2} for Cu (ref. 34) and ~200 mJ m^{-2} for Al (ref. 30) for the unstable stacking) because it results from van der Waals interactions between two layers. This result also qualitatively supports the conclusion that the A–A stacking topological defect should have a transition region much larger than its counterparts in typical metallic systems. To build a mathematical model for an analytic description of the displacement field, we use Fourier transform to get an approximate expression of GSF (more details in the ESI, Section S2†). The result is shown below:

$$\gamma(u,v) = \frac{3A_0{}^2 G_\perp}{2\pi^2 h_0}\left[\cos^2\left(\frac{2\pi u}{3A_0} - \frac{2\pi}{3}\right) + \cos\left(\frac{2\pi v}{\sqrt{3}A_0}\right)\cos\left(\frac{2\pi u}{3A_0} - \frac{2\pi}{3}\right) + \frac{1}{4}\right] \quad (4)$$

where A_0 is the bond length of graphene and h_0 is the inter-layer distance; $G_\perp$ is the effective inter-layer shear modulus. To fit the γ-surface obtained from interatomic potentials, we set $G_\perp$ = 1.588 meV Å^{-3}, A_0 = 1.40 Å and h_0 = 3.34 Å. As shown in Fig. 3(b), the fitting γ-surface matches the directly calculated result very well.

According to eqn (4), the interlayer forces $f_x(u, v) = -\partial_u\gamma/t$ and $f_y(u, v) = -\partial_v\gamma/t$ are nonlinear, so it is difficult to get the analytic solution of the governing equations. But when u, v are small,

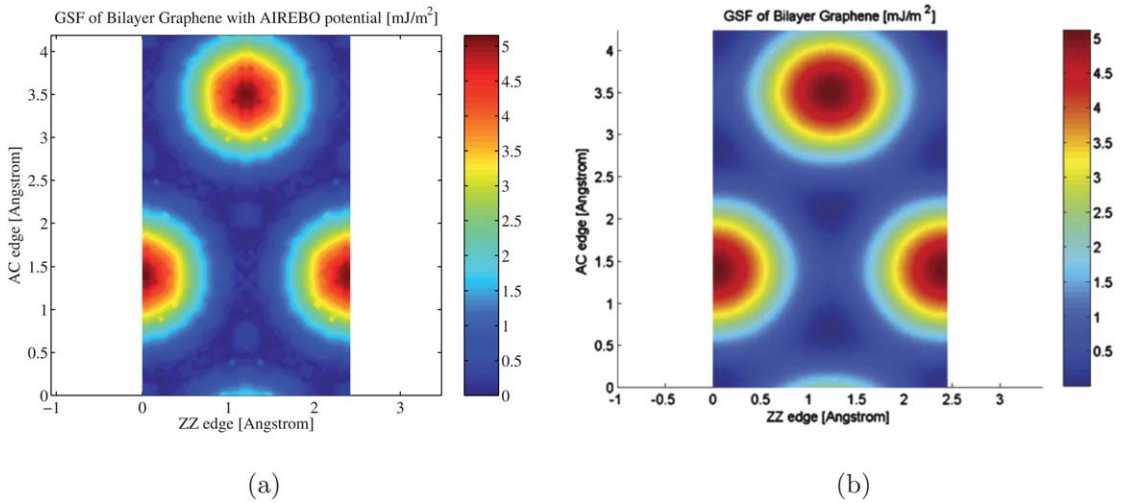

Fig. 3 Generalized stacking fault energy (γ-surface) of BLG. (a) GSF calculated by MD simulation. (b) GSF fitted by eqn (4). ZZ/AC means zigzag/armchair.

which is reasonable for most of the displacement field far away from the center as shown in Fig. 2, we can use the linear perturbation forms of $f_x(u, v)$ and $f_y(u, v)$ instead of the exact nonlinear expressions. Then the governing equations of eqn (3) become

$$\begin{cases} \dfrac{\partial^2 u}{\partial x^2}+\dfrac{1-\nu}{2}\dfrac{\partial^2 u}{\partial y^2}+\dfrac{1+\nu}{2}\dfrac{\partial^2 v}{\partial x\partial y}-k_0{}^2u=-a\delta(x)\delta(y) \\ \dfrac{\partial^2 v}{\partial y^2}+\dfrac{1-\nu}{2}\dfrac{\partial^2 v}{\partial x^2}+\dfrac{1+\nu}{2}\dfrac{\partial^2 u}{\partial x\partial y}-k_0{}^2v=-b\delta(x)\delta(y) \end{cases} \tag{5}$$

where $k_0=\sqrt{\dfrac{2G_\perp(1-\nu^2)}{Eth_0}}$ and $[a, b]$ is the reduced external force, which produces a vector displacement at the origin that is collinear with the force in this linearized isotropic system. Based on these approximate linear interlayer forces, we can adopt Green's function methods to solve eqn (5). There are two displacement fields (u and v), so there are four Green's functions to describe them, two of which are for u and v, respectively. Thus the analytical expressions of the displacement fields can be written in polar coordination as the following

$$\begin{cases} u(r,\theta)=au_1(r,\theta)+bu_2(r,\theta) \\ v(r,\theta)=av_1(r,\theta)+bv_2(r,\theta) \end{cases} \tag{6}$$

Here u_1/u_2 and v_1/v_2 are the Green's functions of the system due to the reduced external force $[a, b]$ at the origin. Mathematically, eqn (6) can be easily solved by using Fourier transform of eqn (5) (more details in the ESI, Section S3†). Their detailed forms are written as follows:

$$\begin{cases} u_1(r,\theta)=\dfrac{1}{2}Q(k_0r)+\dfrac{1}{2}\cos(2\theta)W(k_0r) \\ v_1(r,\theta)=\dfrac{1}{2}\sin(2\theta)W(k_0r) \\ u_2(r,\theta)=\dfrac{1}{2}\sin(2\theta)W(k_0r) \\ v_2(r,\theta)=\dfrac{1}{2}Q(k_0r)-\dfrac{1}{2}\cos(2\theta)W(k_0r) \end{cases} \tag{7}$$

$$\begin{cases} Q(k_0r)=\dfrac{1}{2\pi}{c_f}^2K_0\left(c_fk_0r\right)+\dfrac{1}{2\pi}K_0(k_0r) \\ W(k_0r)=-\dfrac{1}{2\pi}{c_f}^2K_0\left(c_fk_0r\right)+\dfrac{1}{2\pi}K_0(k_0r) \\ \qquad -\dfrac{2}{2\pi}{c_f}^2M\left(c_fk_0r\right)+\dfrac{2}{2\pi}M(k_0r) \\ M(k_0r)=\dfrac{K_1(k_0r)}{k_0r}-\dfrac{1}{(k_0r)^2},\ c_f=\sqrt{\dfrac{2}{1-\nu}} \end{cases} \tag{8}$$

Where $K_0(\cdot)$ and $K_1(\cdot)$ are modified Bessel functions of the second kind. As the linearized eqn (5) gets more accurate compared to the fully non-linear eqn (3) at small u, v, the solution above means that in the far field, the slip corona decays exponentially.

For BLG, $\nu = 0.17$,[35] $Et = 13.89$ eV Å^{-2},[36] and $G_\perp = 1.588$ meV Å^{-3} from the above GSF calculations, therefore we have $k_0 = 0.00814$ Å^{-1}. Under these parameters, the displacement fields $u(x, y)$ and $v(x, y)$ from the analytical solution of eqn (5) are plotted in Fig. 4. Compared with MD results in Fig. 2, the displacements on both the x and y-axes behave almost the same: the larger displacements on the x-axis decay smoothly far from the center, and the smaller displacements on the y-axis behave as the liquid-drop shape in four different sections with different signs. Furthermore, we can find the diameter of this 2D "slip corona" to be about 50 nm, which is exactly what we observed in MD results. Thus, both qualitatively and quantitatively, MD results and analytical solutions match each other. There are only small differences in the center area (diameter ~1 nm), which results from inaccurate linear approximation of nonlinear forces in eqn (5). Thus, for more elaborate study, we must take the nonlinear effects and rippling effects into account to get a more profound understanding. However, this linearized model is good enough to provide some insight into this problem because of its good agreement with MD results in most areas.

C. MD simulations of the BLG nanopore

Beside the ideal defect that only one atom pair is fixed as A–A in a perfect BLG ("point-constraint" case), a more realistic case

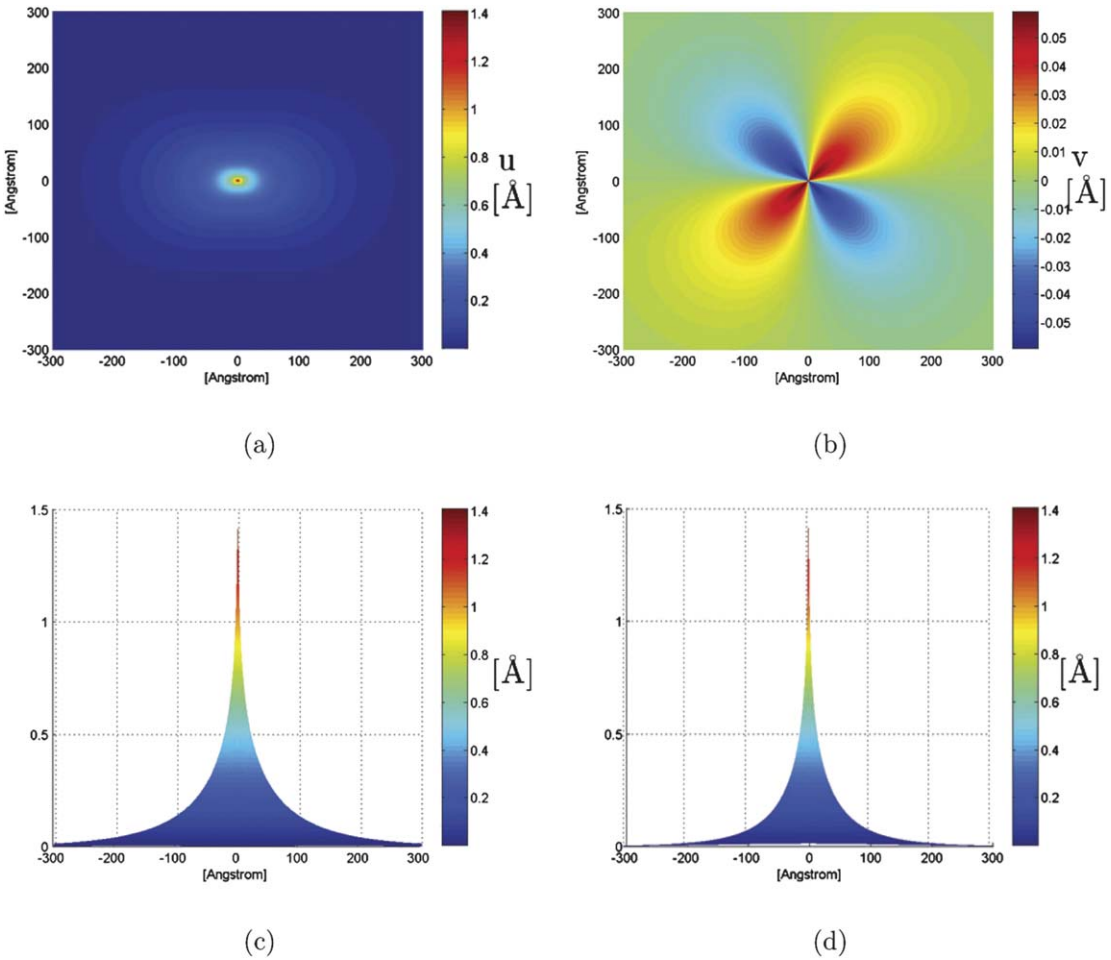

Fig. 4 Continuum model solutions of BLG with single atom pair fixed as A–A stacking. Contours of displacement fields along the x and y-axes, u and v, are shown in (a and b). (c and d) are the total displacement fields ($d = \sqrt{u^2 + v^2}$) projected on the x and y-axes, respectively.

should be the finite-size nanopore with half-nanotube edges as shown in Fig. 1(d). Near BLE there is A–A stacking order locally,[8,9] which would transform into A–B stacking far away. However, the size of the transition area and detailed transition mechanism may be different from the previous "point-constraint" case because there is no artificial force to permanently fix A–A stacking on the BLE. To clarify this effect, we make the same hexagonal nanopore, Fig. 1(d) as described in Section II A. MD simulations were performed to obtain the equilibrium distribution of displacement fields under this configuration.

After relaxation, the atomic structure of the BLG nanopore is plotted in Fig. 5(a) from the top view. Displacement fields along the x- and y-axes are shown in Fig. 5(b) and (c), respectively. Both of them are similar with those of "point-constraint" case except for some deviations. First, for the u field, the maximum value at the center is just ~1.1 Å, less than the carbon–carbon bond length (1.40 Å) in the "point-constraint" case. This is because all the atoms are relaxed and there is no artificial force to fix A–A stacking for any atom pair. On the other hand, this result confirms that BLE makes BLG transition from A–B stacking to the structure close to A–A stacking, even though it can not produce perfect A–A stacking on BLE. Meanwhile, the v field behaves almost the same as its counterpart in the "point-constraint" case (liquid-drop shape in four sections with different signs), except the magnitude increases a little bit (0.08 Å), which may also result from the fact that there is no artificial constraint. Furthermore, the projections of total displacements on both the x and y-axes are plotted in Fig. 5(d). It shows that the slope of maximum displacements decays to almost zero at supercell boundaries, suggesting that the size of transition region has a diameter of ~50 nm, also similar to that of the "point-constraint" case. We also calculate the case of the same hexagonal BLG nanopore in a 100 nm × 100 nm supercell and obtain the same size of the transition region, as shown in the ESI, Fig. S2.† This is because the nanopore has a diameter ~3 nm ≪ 50 nm, so the approximation of "point-constraint" should be correct to describe most area of this slip corona structure. In summary, the high degrees of similarity between the real BLG nanopore and "point-constraint" case support the validity of both solutions.

D. A continuum model of the BLG nanopore

All the above cases are based on the assumption that the size of the nanopore is extremely small so that "point-constraint" approximation is reasonable. When the diameter of the nanopore is comparable with the diameter of this slip corona (~50 nm), the above solution may be not accurate. To illustrate the effect of the nanopore size to slip corona, we use the continuum model to

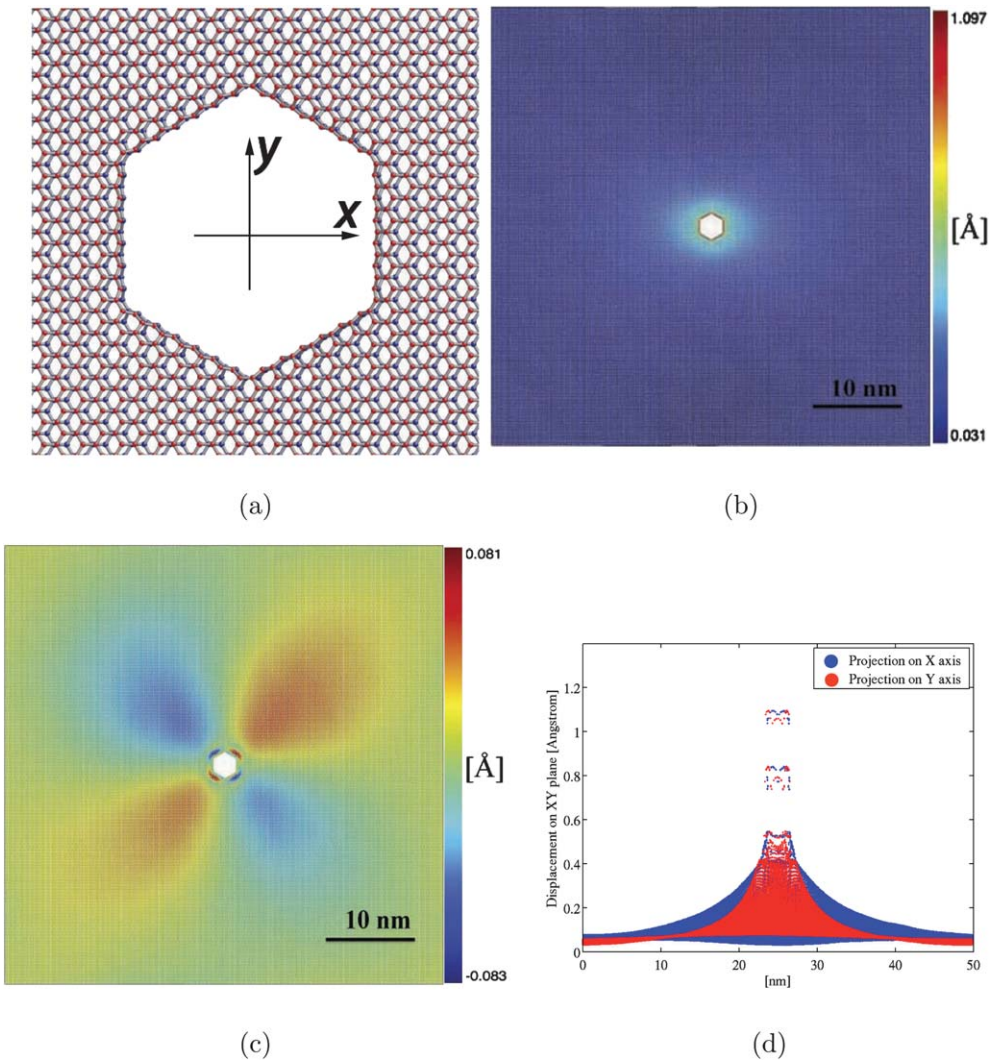

Fig. 5 (a) Top view of the atomic structure of the hexagonal BLG nanopore composed of zigzag BLE after MD relaxation. Red and blue atoms are at the top and bottom layer, respectively. (b and c) Displacement fields along the x (b) and y (c) axes of this hexagonal BLG nanopore in a 50 × 50 nm supercell. (d) Total displacements projected on both the x and y-axes, respectively.

solve the displacement field surrounding the nanopore with various sizes. In principle, we can apply Green's functions of eqn (5) for the BLE nanopore with arbitrary shapes and sizes. If curve ∂C is the BLE surrounding the nanopore, the solution based on Green's functions is

$$\begin{cases} u(x,y) = \iint_C a(x_s,y_s)u_1(r,\theta)\mathrm{d}x_s\mathrm{d}y_s + \iint_C b(x_s,y_s)u_2(r,\theta)\mathrm{d}x_s\mathrm{d}y_s \\ v(x,y) = \iint_C a(x_s,y_s)v_1(r,\theta)\mathrm{d}x_s\mathrm{d}y_s + \iint_C b(x_s,y_s)v_2(r,\theta)\mathrm{d}x_s\mathrm{d}y_s \end{cases}, \quad (9)$$

where (x_s, y_s) is the point in the zone enclosed by the curve ∂C, $r \equiv \left[(x-x_s)^2 + (y-y_s)^2\right]^{\frac{1}{2}}$ and $\theta \equiv \arctan\left(\frac{y-y_s}{x-x_s}\right)$. Because $a(x_s, y_s)$ and $b(x_s, y_s)$ are unknown forces, we cannot get the analytic solution to eqn (9). However, we can get the numerical solution by the following procedure: adopting the orientation of the hexagonal zigzag BLE nanopore as shown in Fig. 5(a), we know $u(x_s, y_s)=A_0$ and $v(x_s, y_s)=0$ within the zone C; so we numerically "invert" the linear system of equations, eqn (9), to get $a(x_s, y_s)$ and $b(x_s, y_s)$ within the zone C; we then substitute these $a(x_s, y_s)$ and $b(x_s, y_s)$ into eqn (9) again, to finally obtain the displacement fields u and v in the whole domain. When the diameter of the nanopore is ~3 nm, the displacement fields of the slip corona, as shown in the ESI, Fig. S5,† are almost the same as those from MD simulations in Fig. 5. Then we increase the diameter of the nanopore gradually and solve the total displacement d along the x-axis. The results are shown in Fig. 6(a), which indicates that the region of the slip corona extends as the size of the nanopore increases. The extreme case is that the diameter of this BLE pore is infinitely large, so each hexagonal edge can be considered as infinitely long zigzag BLE. The displacement field under this limitation can be solved analytically. According to eqn (5), we have $v = 0$ and $\partial_y u = 0$ for the infinitely long zigzag BLE, so eqn (5) becomes

$$\frac{\mathrm{d}^2 u}{\mathrm{d}x^2} - {k_0}^2 u = -a'\delta(x) \quad (10)$$

The solution obviously is $u = A_0\exp(-k_0 x)$ that is also plotted in Fig. 6(a). To make quantitative evaluation, we define the

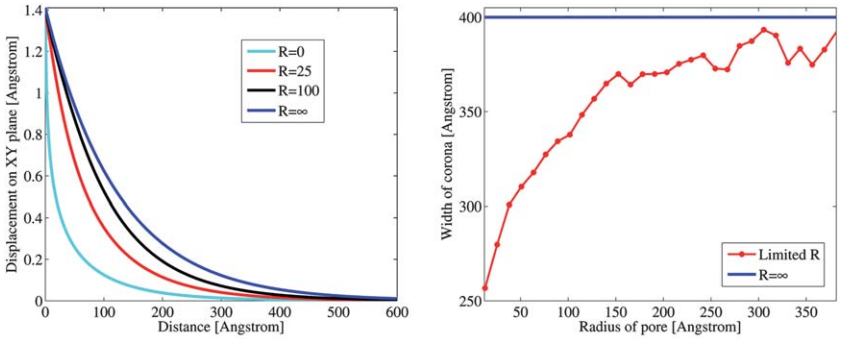

Fig. 6 (a) The total displacements d of BLG along the x-axis defined in Fig. 5(a) for BLE nanopores with various radii ($R \equiv \frac{\sqrt{3}}{2} \times$ edge length). (b) The width of the slip corona *vs.* the radius of the nanopore. The width is defined as the distance from the BLE to the area of almost A–B stacking ($d < 0.05$ Å) along the x-axis in Fig. 5(a).

"width" of the slip corona as the distance from BLE to the area of total displacement smaller than 0.05 Å, and its variation with the size of the nanopore that is plotted in Fig. 6(b), which shows that the width of the slip corona increases gradually with the size (radius) of the nanopore. For the extremely large case as described by eqn (10), the width of the slip corona is ~40 nm. When the diameter of the nanopore is larger than ~80 nm, the width of the slip corona is already convergent to ~40 nm, so it can be considered as the case of infinitely long BLE. On the other hand, for nanopores with a diameter smaller than ~5 nm, the width of the slip corona is still ~25 nm (half of the diameter of the slip corona for the "point-constraint" case), so the "point-constraint" approximation is still valid and the whole slip corona can be roughly regarded as a circular area with a diameter of ~50 nm. Nanopores with such small diameters may have more potential applications in DNA sequencing and molecule/ion selection because of the small sizes of DNA (~2 nm) and molecules/ions.[19–21]

IV. Conclusions

In conclusion, we have demonstrated that a stacking-order transition should happen on the integrated structures of the BLG nanopore from A–A near BLE on the nanopore to A–B far away. We used both MD simulations and the continuum model to reach consistent descriptions of the displacement field $\boldsymbol{s}(x,y)$ between two layers in the transition region in a simple "point-constraint" case; MD simulations of BLG with the real hexagonal nanopore as shown in Fig. 1(d) also output similar $\boldsymbol{s}(x, y)$. The shape of these slip displacement fields is similar to the diffuse corona surrounding the sun and is thereby named "slip corona" on BLG. The size of the "slip corona" (diameter ~50 nm for the extremely small nanopore with the diameter $D_{\text{pore}} < 5$ nm) is much larger than the width of the typical dislocation core (~1 nm) in 3D metals or the nanopore itself, due to the weak van der Waals interactions and low interlayer shear resistance between two adjacent layers of graphene. The continuum model also suggests that the width of this "corona" from the BLE to the A–B stacking area would increase gradually as D_{pore} increases and converge to ~40 nm as D_{pore} reaches to ~80 nm.

The slip displacement between two layers in BLG can significantly change the band structure near the Dirac point,[37] and an inhomogeneous displacement field $\boldsymbol{s}(x, y)$ can bring more interesting results. For example, BLG with a small angle rotation between two layers, which also produces a stacking defect, was found not to open an electronic gap under an external electric field perpendicular to the layers.[13] Here our BLG nanopore with slip corona could result in new electronic and optical properties since it significantly changes the local symmetry and introduces a relatively large continuum field to the lattice structure. In addition, we can produce arrays of BLG nanopores on a large BLG, with associated slip coronas interfering constructively or destructively with each other. We note that each slip corona carries a "vector charge" **BA** or Burgers vector with three possibilities as shown in Fig. 1(a). The total displacement fields would depend on the density, position and vector charge arrangements of such arrays and the size of an individual nanopore, which may provide us with a new avenue to produce graphene-based devices like the concept of metamaterials.[38]

Acknowledgements

LQ and JL acknowledge support by AFOSR FA9550-08-1-0325. YWM acknowledges support by 973 Programs of China (2010CB631003, 2012CB619402).

References

1 E. V. Castro, K. S. Novoselov, S. V. Morozov, N. M. R. Peres, J. M. B. L. Dos Santos, J. Nilsson, F. Guinea, A. K. Geim and A. H. C. Neto, *Phys. Rev. Lett.*, 2007, **99**, 216802.
2 Y. Zhang, T.-T. Tang, C. Girit, Z. Hao, M. C. Martin, A. Zettl, M. F. Crommie, Y. R. Shen and F. Wang, *Nature*, 2009, **459**, 820.
3 T. Ohta, A. Bostwick, T. Seyller, K. Horn and E. Rotenberg, *Science*, 2006, **313**, 951.
4 K. Novoselov, E. McCann, S. Morozov, V. Fal'ko, M. Katsnelson, U. Zeitler, D. Jiang, F. Schedin and A. Geim, *Nat. Phys.*, 2006, **2**, 177.
5 E. McCann and V. Fal'ko, *Phys. Rev. Lett.*, 2006, **96**, 086805.
6 E. McCann, *Phys. Rev. B: Condens. Matter Mater. Phys.*, 2006, **74**, 161403.
7 Z. Liu, K. Suenaga, P. J. F. Harris and S. Iijima, *Phys. Rev. Lett.*, 2009, **102**, 015501.
8 J. Y. Huang, F. Ding, B. I. Yakobson, P. Lu, L. Qi and J. Li, *Proc. Natl. Acad. Sci. U. S. A.*, 2009, **106**, 10103.

9 J. Feng, L. Qi, J. Y. Huang and J. Li, *Phys. Rev. B: Condens. Matter Mater. Phys.*, 2009, **80**, 165407.
10 J. Feng, W. B. Li, X. F. Qian, J. S. Qi, L. Qi and J. Li, *Nanoscale*, 2012, **4**, 4883.
11 A. H. Castro Neto, F. Guinea, N. M. R. Peres, K. S. Novoselov and A. K. Geim, *Rev. Mod. Phys.*, 2009, **81**, 109.
12 P. M. Ostrovsky, I. V. Gornyi and A. D. Mirlin, *Phys. Rev. B: Condens. Matter Mater. Phys.*, 2006, **74**, 235443.
13 J. M. B. L. dos Santos, N. M. R. Peres and A. H. Castro Neto, *Phys. Rev. Lett.*, 2007, **99**, 256802.
14 R. V. Gorbachev, F. V. Tikhonenko, A. S. Mayorov, D. W. Horsell and A. K. Savchenko, *Phys. Rev. Lett.*, 2007, **98**, 176805.
15 L. Qi, J. Y. Huang, J. Feng and J. Li, *Carbon*, 2010, **48**, 2354.
16 J. S. Qi, J. Y. Huang, J. Feng, D. N. Shi and J. Li, *ACS Nano*, 2011, **5**, 3475.
17 Y. Zhu, S. Murali, M. D. Stoller, K. J. Ganesh, W. Cai, P. J. Ferreira, A. Pirkle, R. M. Wallace, K. A. Cychosz and M. Thommes, *et al.*, *Science*, 2011, **332**, 1537.
18 J. Xiao, D. Mei, X. Li, W. Xu, D. Wang, G. L. Graff, W. D. Bennett, Z. Nie, L. V. Saraf and I. A. Aksay, *et al.*, *Nano Lett.*, 2011, **11**, 5071.
19 K. Sint, B. Wang and P. Kral, *J. Am. Chem. Soc.*, 2008, **130**, 16448.
20 R. R. Nair, H. A. Wu, P. N. Jayaram, I. V. Grigorieva and A. K. Geim, *Science*, 2012, **335**, 442.
21 S. Garaj, W. Hubbard, A. Reina, J. Kong, D. Branton and J. A. Golovchenko, *Nature*, 2010, **467**, 190.
22 C. A. Merchant, K. Healy, M. Wanunu, V. Ray, N. Peterman, J. Bartel, M. D. Fischbein, K. Venta, Z. Luo and A. T. C. Johnson, *et al.*, *Nano Lett.*, 2010, **10**, 2915.
23 G. F. Schneider, S. W. Kowalczyk, V. E. Calado, G. Pandraud, H. W. Zandbergen, L. M. K. Vandersypen and C. Dekker, *Nano Lett.*, 2010, **10**, 3163.
24 S. K. Min, W. Y. Kim, Y. Cho and K. S. Kim, *Nat. Nanotechnol.*, 2011, **6**, 162.
25 J. P. Hirth and J. Lothe, *Theory of Dislocations*, Krieger Pub. Co., May 1992.
26 R. Peierls, *Proc. Phys. Soc.*, 1940, **53**, 34.
27 F. R. N. Nabarro, *Proc. Phys. Soc.*, 1947, **59**, 256.
28 V. Vitek, *Philos. Mag.*, 1968, **18**, 773.
29 B. Joos, Q. Ren and M. Duesbery, *Phys. Rev. B: Condens. Matter Mater. Phys.*, 1994, **50**, 5890.
30 G. Lu, N. Kioussis, V. Bulatov and E. Kaxiras, *Phys. Rev. B: Condens. Matter Mater. Phys.*, 2000, **62**, 3099.
31 S. Stuart, A. Tutein and J. Harrison, *J. Chem. Phys.*, 2000, **112**, 6472.
32 A. Fasolino, J. H. Los and M. I. Katsnelson, *Nat. Mater.*, 2007, **6**, 858.
33 L. Landau, E. Lifchits and A. Kosevitch, *Theory of Elasticity*, Pergamon Press, 1986.
34 S. Ogata, J. Li and S. Yip, *Science*, 2002, **298**, 807.
35 G. Gui, J. Li and J. Zhong, *Phys. Rev. B: Condens. Matter Mater. Phys.*, 2008, **78**, 075435.
36 J. Atalaya, A. Isacsson and J. M. Kinaret, *Nano Lett.*, 2008, **8**, 4196.
37 K. Kim, Z. Lee, B. D. Malone, K. T. Chan, B. Aleman, W. Regan, W. Gannett, M. F. Crommie, M. L. Cohen and A. Zettl, *Phys. Rev. B: Condens. Matter Mater. Phys.*, 2011, **83**, 245433.
38 A. Vakil and N. Engheta, *Science*, 2011, **332**, 1291.